13

Boron based x-ray multilayer mirrors for the spectral range 6.7−9 nm

© R.A. Shaposhnikov, N.V. Zagaynov, V.N. Polkovnikov, N.I. Chkhalo, S.A. Garakhin, S.Yu. Zuev

Institute for physics of microstructure RAS,
603087 Nizhny Novgorod, Russia
e-mail: shaposhnikov-roma@mail.ru

Received April 12, 2024
Revised April 12, 2024
Accepted April 12, 2024

The paper presents the results of a study of the reflective characteristics and structural parameters of multilayer X-ray mirrors based on a pair of Ru/B4C materials, optimized for the spectral range 67−90 Å. A comparison of these structures with Mo/B_4C and La/B_4C mirrors is presented.

Keywords: multilayer X-ray mirrors, synchrotron applications, X-ray monochromators, X-ray lithography.

DOI: 10.61011/TP.2024.08.59003.119-24

Introduction

The projection lithography is one of the most important practical applications of multilayer X-ray mirrors (MLMs). At the moment, 193 nm projection lithography is the main method used in the production of microchips. However, 13.5 nm lithography (EUV-extreme ultraviolet) has been used in recent years to produce critical layers with minimal dimensions. Spatial resolution and performance are important characteristics of a lithograph.

In compliance with the Rayleigh criterion, the minimum allowed object size is

$$a_{\min} = \frac{k \cdot \lambda}{NA}, \quad (1)$$

where k is the proportionality coefficient (of the order of one) associated with the properties of the radiation source and the method of mask illumination, NA is the numerical lens aperture, λ is the radiation wavelength. It is possible either to increase NA, or to use shorter operating wavelengths for improving the spatial resolution. The first option is more related to the technological difficulties of manufacturing the appropriate lens [1]. We consider only the second option in this paper.

The system performance, in turn, depends on the power and spectral characteristics of the radiation source, as well as the reflective properties of the multilayer mirrors used to design the optical scheme of the lithographing printer.

In practice, the following ratio is used to correctly compare the efficiency of various sources and optical systems, taking into account the spectral bandwidth of the optical system [2]:

$$E = R^{10} S(\lambda)\Delta\lambda = R^{10} CE, \quad (2)$$

where CE is conversion rate, which characterizes the proportion of total energy consumed by the source (for example, the energy of laser radiation incident on the target) that is emitted into half-space in the spectral bandwidth of the optical system, performance λ is the operating wavelength, $R(\lambda)$ is the dependence of the reflection coefficient on the MLMs wavelength in the optical scheme of the lithographing printer (degree 10 corresponds to a system consisting of 10 mirrors). So CE depends on the source properties and system bandwidth.

Given the above, it is possible to conclude that the choice of the operating wavelength for lithography should be made based on two factors: the presence of multilayer X-ray mirrors with high reflection coefficients at the operating wavelength, as well as the presence of effective radiation sources. It is these factors that determine the choice of a promising operating wavelength of next-generation lithography.

Currently, the projection lithography is used for the production of microchips at an operating wavelength of 135 Å. NXE:3400 series lithography systems from ASML, the Netherlands are used for this purpose [3]. The analysis of the properties of radiation sources and multilayer structures shows that a wavelength in the vicinity of 67 Å can be a promising wavelength for next-generation lithography. Firstly, boron absorption K-edge ($\lambda_K \sim 66.3$ Å) is located in this spectral region, which makes it possible to choose this material as a weakly absorbing material for the synthesis of effective MLMs based on it [4]. Secondly, sources based on terbium and gadolinium [5,6] can ensure high effective system power. Thirdly, according to the formula (1), switching to a given wavelength with the same value of NA allows for a twofold increase of the resolution compared to the actively developed lithography with an operating wavelength of 135 Å.

Another important practical application of MLMs optimized for the operating wavelength of 67 Å is X-ray fluorescence analysis, which is a non-destructive method for examination of the studied objects. This method can be used, for example, for measuring the concentration of boron impurities in diamond [7], which is an important task for the development of diamond electronics. The source radiation in this method is focused on the sample

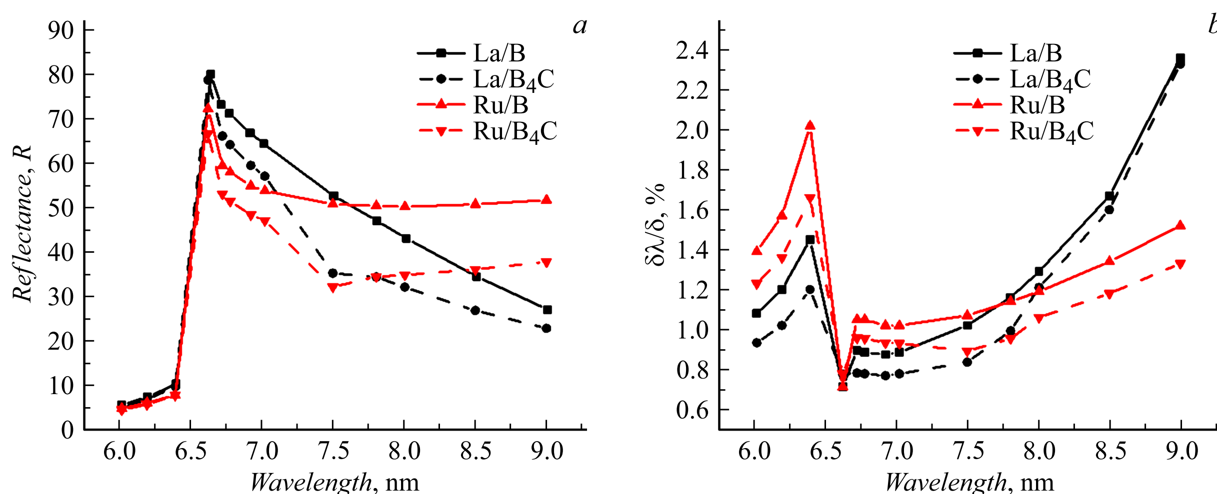

Figure 1. The dependence of reflection coefficient (*a*) and spectral selectivity (*b*) for ideal structures La/B (black solid curve), La/B_4C (black dashed line curve), Ru/B (red solid curve), Ru/B_4C (red dashed curve) in the range of 6–9 nm at a radiation grazing angle of 90 deg.

using a monochromator mirror, which allows selecting the operating wavelength from the radiation spectrum. Next, the monochromatic radiation reflected from the first mirror hits the sample, which results in the ionization of the atoms. Part of the fluorescent radiation released from the sample is captured by the second monochromator mirror and focused on the detector entrance slit. The analysis of the radiation received by the detector results in a conclusion about the atomic composition of the studied sample. It is necessary to provide the maximum possible reflection coefficient of multilayer mirrors in the optical circuit for effective operation of the device.

Another practical application of MLMs is development of monochromators for synchrotron radiation stations, where MLMs are used as optical elements that ensure the beam monochromatization [8]. In this case, it is necessary to ensure not only a high reflection coefficient, but also a high degree of radiation monochromatization ($\Delta\lambda/\lambda$ usually better than 1%), and in a wide spectral range. This results in the need to synthesize structures with a narrow bandwidth, as in the case of using multilayer X-ray mirrors in spectroscopy problems [9].

In order to use MLMs as reflective elements in the optical circuit of the lithograph, it is necessary that they ensure the highest possible integral (i.e., taking into account the spectral bandwidth) reflection coefficient, since the time of photoresist illumination and, consequently, the time spent on chip production depends on it. Spectroscopy tasks, on the contrary, require the narrowest possible spectral width of the reflection peak.

Fig. 1 shows the theoretical dependences of the peak value of the reflection coefficient (Fig. 1, *a*) and the spectral bandwidth (Fig. 1, *b*) for ideal (i.e., without roughness and with tabular values of material densities) MLMs based on various materials in the range from 60 to 90 Å.

It can be seen from the presented dependences that the highest peak reflection coefficient of 80% (in the neighborhood of the wavelength of 67 Å) allows obtaining structures based on a pair of lanthanum and boron materials. Replacing boron with optically close boron carbide reduces the reflection coefficient for all considered structures. Mirrors based on Ru can achieve higher reflection coefficients than structures based on La at operating wavelengths greater than 78 Å. This range is interesting both for X-ray fluorescence analysis and for creating monochromators at synchrotron stations. Thus, mirrors based on La and Ru can be considered as promising for solving a number of practical problems.

The most studied MLMs are based on La. It is important to note that the currently known experimentally obtained reflection coefficients for La/B and La/B_4C multilayer X-ray mirrors are significantly inferior to the theoretical ones. One of the main factors determining the difference between experimental and theoretical results is the presence of extended boundaries between layers because of the mutual diffusion and chemical activity of materials, as well as the presence of interlayer roughness in structures. The reflection coefficient R = 40% at a wavelength of 66.6 Å for a La/B_4C multilayer mirror with a period of $d = 33.5$ Å was obtained in the paper[10].

Another method for reducing the size of interfaces is the nitration of La layers, which can be carried out by injection of N_2 gas during structure synthesis. The reflection characteristics of La/B_4C, LaN/B_4C and $La/C/B_4C$ structures optimized for the operating wavelength of 67 Å were studied in the article [12]. For La/B_4C: $R = 51.1\%$ at an angle of incidence of 10 deg and period of $d = 34$ Å. For LaN/B_4C: $R = 58.1\%$ at an angle of incidence of 10 deg and period of $d = 34$ Å. It follows from the results obtained that nitridization of La layers significantly increased the reflection coefficient. The addition of carbon interlayers

also increased the reflectivity of the structures. A reflection coefficient of 58.6% was obtained for La/B_4C/C-structures at a wavelength of 66.6 Å at a grazing angle of 69.1 deg when carbon layers with thickness of 2.5=3 Å were deposited on the more extended La-on-B_4C boundary.

The best results in terms of reflection coefficient for lanthanum-based mirrors were obtained in Ref. [13]. The authors present the value of the reflection coefficient of $R = 64.1\%$ for LaN/B structures at an angle of incidence of 1.5 deg from the normal and a wavelength of 66.5 Å.

It is worth noting that at the moment the value of the reflection coefficient presented above is a record among those obtained experimentally. At the same time, it is significantly lower than the theoretically possible limit of $R_{\text{th}} = 80\%$. It can be noted that there are no data in the literature about the reflectivity of La/B and La/B_4C mirrors in the wavelength range of $\lambda > 67$ Å.

The question of ruthenium-containing mirrors is less studied. There is a relatively small number of papers on Ru/B_4C structures, and there is no information about Ru/B structures. At the same time, even for Ru/B_4C, there is no data on reflectivity in the considered spectral range.

The effect of annealing on Ru/B_4C nd Ru/C structures with periods $d = 35$ Å was studied in paper [14]. It is shown that annealing at a temperature of 600°C for 1 h resulted in an increase of the roughness of Ru/C structures, while the roughness of Ru/B_4C structures practically did not change.

The effect of annealing at a temperature of 200°C on the internal stresses of Ru/B_4C structures is studied in Ref. [15]. It was shown that an increase of the annealing time results in a decrease of the internal stresses at any fraction of ruthenium in the structure period.

The effect of annealing on Ru/B_4C structures with periods of $d = 39$ Å was studied in Ref. [16]. The measurement of the angular dependence of the reflection coefficient at a radiation energy of 20 keV showed no decrease of the reflection coefficient in the first Bragg peak during annealing of the structure at 550°C.

Ru/B_4C structures synthesized in a mixture of argon and nitrogen were studied in Ref. [17]. It was shown that the addition of nitrogen can significantly reduce internal stresses in the structure and increase the reflection coefficient. For instance, the structures synthesized at a nitrogen partial pressure of 15% had almost zero stress (−28 MPa) and a significantly higher reflection coefficient — 67% with an emission energy of 8.04 keV, while the reflection coefficient of structures synthesized in pure argon was 54%.

It is worth noting that Ru/B_4C-structures were studied in the field of hard X-ray radiation in the above papers. However, the question of synthesis and investigation of multilayer mirrors based on ruthenium in the soft X-ray wavelength range remains open.

The reflective properties and structural parameters of Ru/B_4C MLMs were studied in this paper.

1. Experimental method

The multilayer mirrors studied in this paper were synthesized by magnetron sputtering on the facility [18], the diagram of which is shown in Fig. 2.

This installation is a cylindrical vacuum chamber with a height of 0.5 m and a diameter of 0.8 m, provided with four planar magnetrons. The targets of sputtering materials are located at the magnetrons. During the process, the substrate passes over each magnetron in turn, which allows up to 4 different materials to be applied layer-by-layer in a single structure during a single workflow. There are shaped diaphragms between the substrate and the magnetrons. The shape of the diaphragms determines the distribution of the sputtered material on the substrate. Depending on the tasks, it may be necessary to ensure both a uniform distribution of the material over the surface and a distribution with a given law. The substrate is circularly moved by a stepper motor. The speed of passing the substrate over the magnetrons allows determining the thickness of the layer applied to the substrate in one pass. The magnetrons are powered by stabilized current sources developed by IPM RAS. Discharge currents can vary from 100 to 1200 mA, and the voltage is usually 200−400 V. Mirrors are synthesized under the pressure of residual gases in the vacuum volume at the level of 10^{-7} Torr. The atmospheric gases entering the vacuum volume results in rapid degradation of targets when such chemically active materials as strontium and lanthanum are used. The problem of synthesis of high-quality structures based on boron carbide also occurs when atmospheric air is introduced into the working volume. The facility was provided with a special vacuum lock, separated by a vacuum lock from the main volume for solving the above problems.

The reflectance characteristics of the synthesized samples were measured using a Panalitical X'Pert PRO four-crystal diffractometer, which allows studying structures by small-angle diffraction method. In addition to measuring the

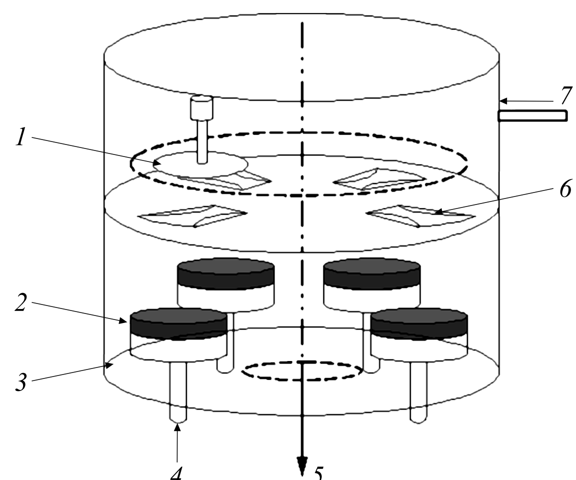

Figure 2. Experimental setup diagram: *1* — substrate with motor, *2* — target, *3* — magnetron, *4* — cooling, *5* — pumping system, *6* — shaped apertures, *7* — argon supply to the camera.

reflectance characteristics of the studied structures in the hard X-ray range ($\lambda = 1.54$ Å), reflection coefficients were also measured in the soft X-ray range at wavelengths of $\lambda = 9.89$, 17.59, 93.4 A on a laboratory reflectometer, provided with monochromator RSM-500 [19].

The structural parameters of the synthesized samples were determined using a technique implemented in the Multifitting software product developed by IPM RAS [20]. This program allows calculating the spectral and angular dependences of the reflection coefficient on the model structure by solving a system of recurrent relations, as well as performing simultaneous fitting of several experimental curves taken in different spectral ranges. The greater the number of curves simultaneously processed by the program, the closer to the real ones will be the obtained values of the model structure parameters. Therefore, a simultaneous fitting of reflection curves measured in both hard and soft X-ray regions is usually performed to determine the structural parameters of the synthesized sample. Period, material thicknesses per period, transition region widths, and material densities are the parameters of the structure determined during fitting. It is possible to calculate the reflection characteristics of the structure in other spectral and angular ranges based on the obtained structural parameters.

One of the main advantages of this program is taking into account the blurring of layer boundaries in the structure (interlayer interfaces), which is set through the superposition of functions of the dependence of the dielectric permittivity profile on the coordinate deep into the sample. In addition to mirror curves, it is also possible to analyze diffuse scattering curves in the Multifitting program to separate the contributions of layer mixing and geometric roughness to the reflection curves.

In addition to the reflective properties of Ru/B_4C MLMs, their mechanical properties were also studied in this paper. Specifically, the internal stresses that occur in structures during growth.

Almost all films are in a state of tension regardless of the method of their production. Stresses in a film (solid or multilayer) can be tensile when the film seems to try to contract on the substrate — the force counteracts compression, „stretches“ film and is directed from the center of the substrate to the periphery. In this case, it is customary to assign the sign „plus“ to the value of internal stresses. Stresses can also have a compressive character, i.e. forces are directed from the periphery to the center. Then it is customary to talk about negative voltages and assign „minus“ to them. The film + substrate system has a concave character with the sign „plus“ it has a convex character with the sign „minus“ with the film directed outward. The presence of internal stresses in multilayer structures can result in deformations of the shape of optical elements, which, in turn, can result in a deviation of the beam path from the calculated one.

The Stoney formula is used to determine internal stresses

$$\sigma = \frac{E}{6(1-\nu)} \frac{d_{\text{sub}}^2}{d_f} \left(\frac{1}{R_2} - \frac{1}{R_1} \right), \tag{3}$$

where σ — stress, E — Young's modulus of the plate material, ν — Poisson's ratio of the plate material, d_{sub} — substrate thickness, d_{f} — film thickness, R_1 — initial radius of curvature of the substrate, R_2 — radius of curvature of the substrate after film deposition. Thus, the problem is reduced to measuring the radius of curvature of the initial surface and the radius of curvature of the surface after application of a multilayer structure to it.

Determination of the radii of curvature of substrates before sputtering and coated substrates after sputtering was carried out by the interferometric method using laser interferometer Zygo VeriFire 4. The method for measuring internal stresses is described in more details in Ref. [21].

2. Results and discussion

The theoretical calculation of the dependence of the reflection coefficient on the parameter β was the first stage of studies of multilayer structures Ru/B_4C, which is defined as the ratio of the thickness of a highly absorbing material in the period to the value of the period. In this case $\beta = d_{\text{Ru}}/d$, where d_{Ru} — the thickness of ruthenium in the period of the structure, d — the period of the multilayer mirror. The calculation was performed for ideal structures with zero interlayer roughness, no period drift, and tabular values of material densities. $N = 200$ was chosen as the number of periods in this calculation. An increase of the number of layers does not result in an increase of the reflection coefficient due to the absorption of incident radiation by the structure. This calculation of the dependence $R(\beta)$ is shown in Fig. 3. The period of structures $d = 33.7$ Å, which corresponds to the case of normal radiation incidence at a wavelength of 67 Å. Respectively the value of reflections in Fig. 3 is provided for this wavelength.

It is possible to conclude from the presented dependence that the maximum theoretically possible reflection coefficient is $R = 56\%$ and is reached at the values $\beta = 0.3-0.35$. The reflection coefficient begins to fall when this parameter decreases or increases relative to the optimal value. It should also be noted that the drop of the reflection coefficient is not significant in the range of $\beta = 0.25-0.4$ and is about 2%.

The synthesis of Ru/B_4C multilayer structures and the study of their structural parameters was the next stage of the study. A set of Ru/B_4C MLMs with periods of about 34–35 Å and various values of β was studied in this paper. Their structural parameters are shown in the table.

The parameters shown in the table are obtained by fitting the reflection curves taken at wavelengths of 1.54, 9.89, and 17.59 Å. Fig. 4 shows an example of such a fitting for a sample with $\beta = 0.45$. Experimental dependences of the reflection coefficient on the radiation grazing angle for the

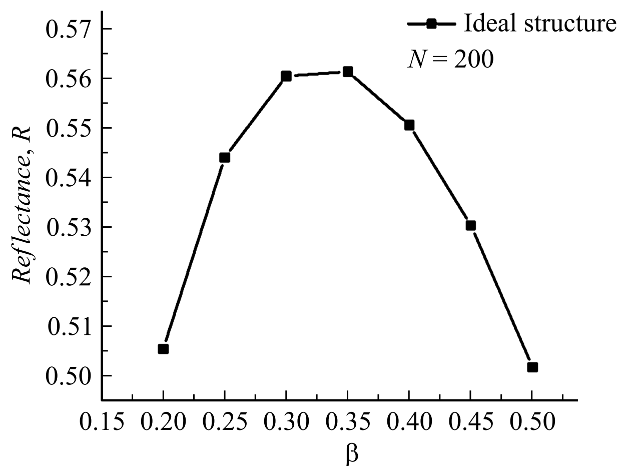

Figure 3. Theoretical dependence of the reflection coefficient of an ideal Ru/B_4C MLMs on the parameter $\beta = d_{Ru}/d$ at a wavelength of 67 Å.

Structural parameters of the studied samples

Period, Å	β	S_Ru, Å	S_B_4C, Å
34.45	0.6	1.9	1.9
34.55	0.45	2.3	2.3
35.45	0.33	2.2	2

Note. S_Ru and S_B4C — transition layer widths at the B_4C-to-Ru and Ru-to-B_4C boundaries, respectively.

wavelengths of $\lambda = 1.54$, 9.89, 17.59 Å, as well as fitting of experimental data.

Fig. 5 shows the reconstructed profiles of the real part of the dielectric permittivity allowance δ (where $\varepsilon = 1 - \delta + i\gamma$, ε — dielectric permittivity) for samples with $\beta = 0.6$ (Fig. 5, *a*), 0.45 (Fig. 5, *b*), and 0.3 (Fig. 5, *c*).

The fitting of the experimental data allowed determining that the values of the transition regions are 2.3 Å for both boundaries. These values of the width of the transition regions are obtained as follows. In case of fitting of experimental data, the transition region profile is defined by a linear combination of functions with different weight coefficients. The value of the width of the transition area, which is given in this paper, is included in these functions as an argument. The error function and linear function were used in this paper. The explicit form of functions is given in the paper [20]. These values correspond to those obtained earlier for the Mo/B_4C [22]. Meanwhile, the Ru/B_4C material pair has better optical characteristics to maximize the reflection coefficient than Mo/B_4C in the wavelength range of 6.7–9 nm. Therefore, we can conclude that Ru/B_4C-structures can be a good alternative to mirrors based on Mo/B_4C.

The values of the width of transition layers determined during fitting are quite low, which eliminates the need for using interface engineering techniques in contrast to La/B_4C-structures.

The obtained parameters allow for a theoretical prediction of the values of reflection coefficients for MLMs Ru/B_4C

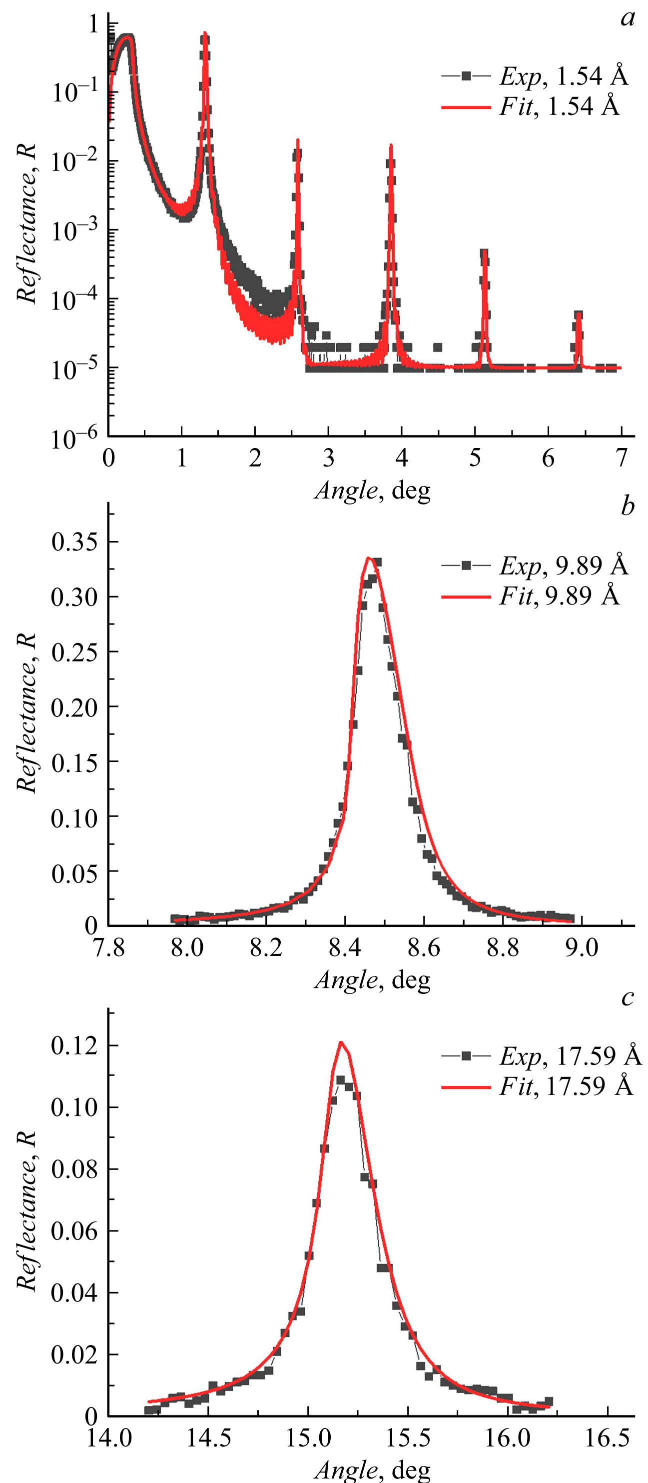

Figure 4. Experimentally measured dependences of the reflection coefficient (black curves) on the radiation grazing angle and their fitting (red curves) for the wavelengths of $\lambda = 1.54$ (*a*), 9.89 (*b*) and 17.59 Å (*c*).

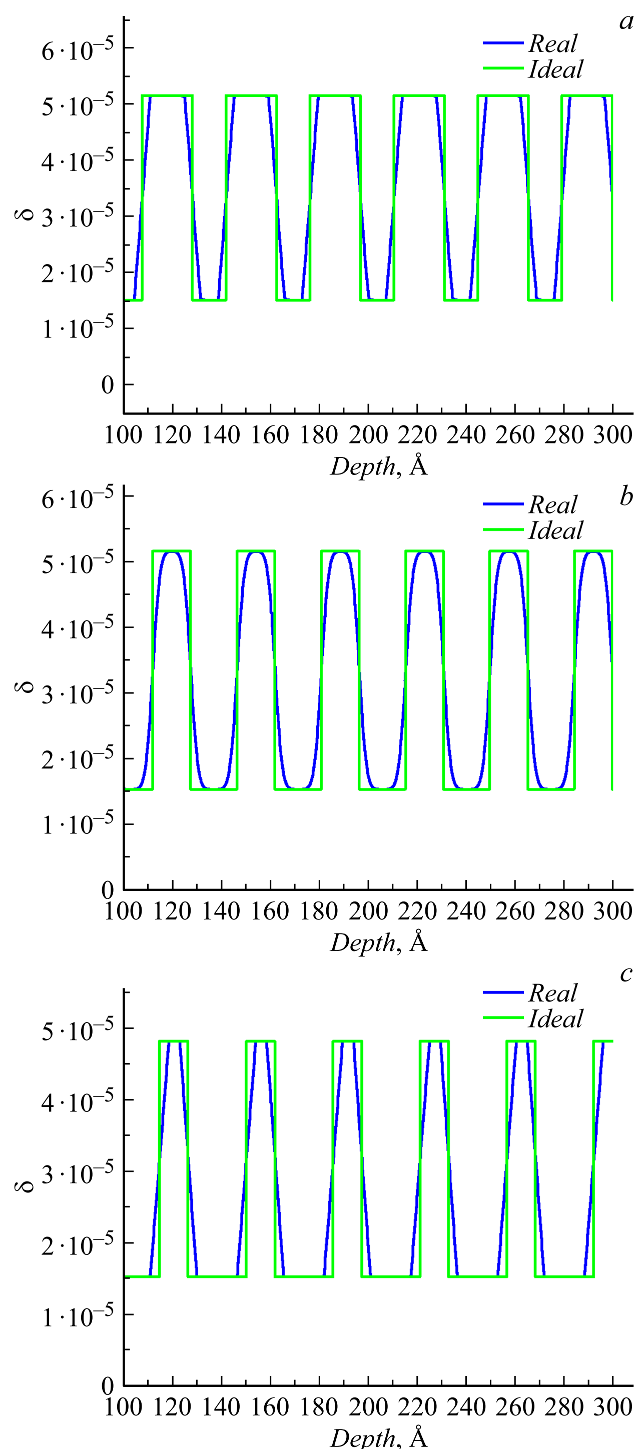

Figure 5. Profiles of the real part of the dielectric permittivity allowance for a real structure with interlayer interfaces (blue curve) and for an ideal structure with zero transition region width (green curve).

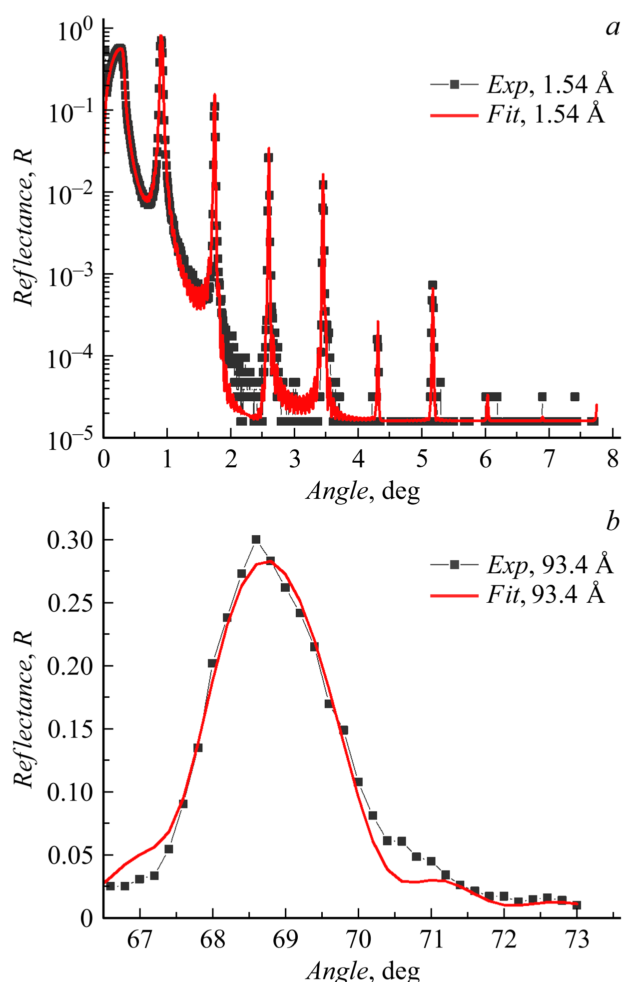

Figure 6. Experimentally measured (black curves) and theoretically calculated (red curves) dependences of the reflection coefficient on the grazing angle for the wavelengths of 1.54 (*a*) and 93.4 Å (*b*), taking into account the reconstructed structural parameters.

in a wide spectral range. We demonstrated this using the example of the Ru/B_4C MLMs with a period of 51.4 Å. A comparison of experimentally obtained reflection coefficients and theoretically calculated reflection coefficients based on previously obtained structural parameters for the Ru/B_4C MLMs with a period of 51.4 Å is shown in Fig. 6. Reflection is obtained for $\lambda = 1.54$ and 93.4 Å.

A good match of the experimental and theoretically predicted curves is seen.

Fig. 7 shows the diffuse scattering curve taken at the first Bragg peak for a structure with parameters $N = 150$ (number of periods), $d = 34.55$ A (period value), $\beta = 0.45$ (ruthenium fraction in the period). The joint analysis of diffuse scattering and specular reflection curves makes it possible to distinguish between geometric roughness resulting from deformation of the boundary between layers of different materials as a whole, and diffuse roughness resulting from mixing of materials at the boundary due to atomic diffusion and chemical interaction. It was assumed in the framework of the selected model that the geometric roughness is the same for both boundaries. A linear growth model [23,24] was chosen to calculate the boundary roughnesses, within which the PSD (power spectral density)

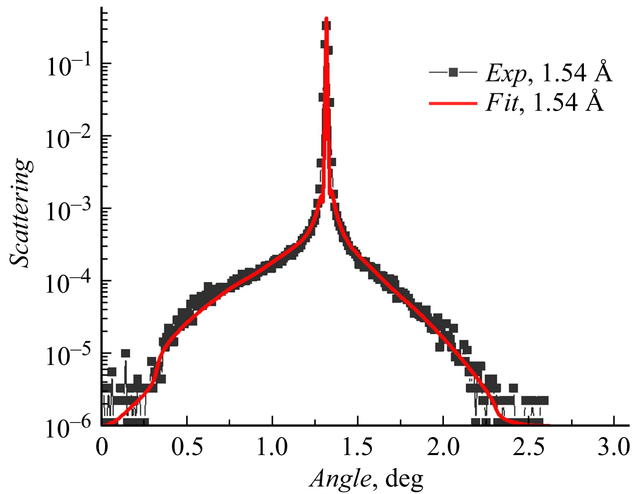

Figure 7. Experimental diffuse scattering curve (black curve) taken at the first Bragg peak and its fitting (red curve.)

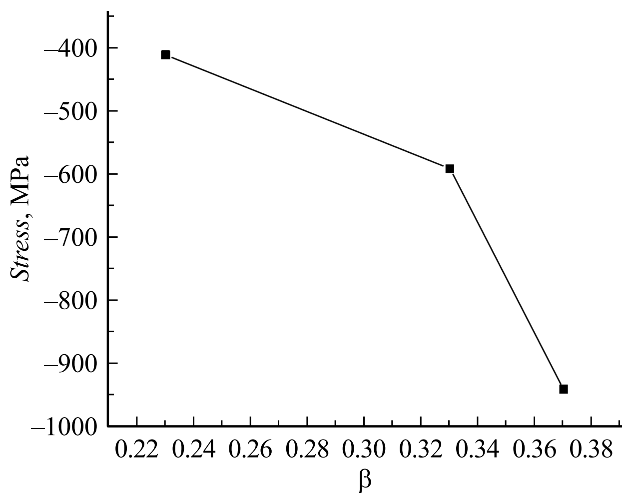

Figure 8. The dependence of internal stresses on the proportion of ruthenium in the period.

function of the interfaces is partially inherited from previous ones and partially replaced by a growth model:

$$\mathrm{PSD}_{2D}(\nu) = \mathrm{PSD}_{\mathrm{sub}}(\nu)e^{-b(\nu)h} + \Omega\frac{1 - e^{-b(\nu)h}}{e^{-b(\nu)h}},$$

where $\mathrm{PSD}_{\mathrm{sub}}(\nu)$ corresponds to the substrate, $e^{-b(\nu)h}$ — inheritance factor, Ω — volume of the deposited particle (atom, molecule, or cluster), h — film thickness, $b(\nu)$ — surface relaxation function, ν — spatial frequency. The ABC model was chosen as the model describing the PSD function of the substrate [24]. The PSD function of the substrate has the following form

$$\mathrm{PSD}_{\mathrm{sub}}(\nu) = \frac{4\pi\sigma^2\xi^2\alpha}{(1 + \xi^2(2\pi\nu)^2)^{\alpha+1}},$$

where σ —full RMS roughness α — fractal dimension that determines the rate at which the spectrum decays to high frequencies, ξ — cross-correlation length (the cross-correlation length, i.e. along the layer).

The layer roughness value was obtained by integrating the PSD function in a given spatial frequency range, which was determined from the following condition: $2\pi\nu = k(\cos\vartheta_0 - \cos\vartheta)$, where ν — the value of the spatial frequency, ϑ_0 — the angle corresponding to the specular reflection, ϑ — the scattering angle, k — wave vector. The value of the scattering angle close to the Bragg peak was chosen as the lower boundary of integration, and the value corresponding to the angle of maximum scattering was chosen as the upper boundary.

It follows from the presented data that the value of the geometric roughness is $\sigma = 0.74$ Å.

The dependence of internal stresses measured for a number of synthesized structures by the interferometric method on the fraction of ruthenium in the period of a multilayer mirror is shown in Fig. 8. Several conclusions can be drawn based on the data presented. Firstly, internal stresses have a negative sign over the entire range of the studied parameter β. Secondly, the value of internal stresses increases modulo with increasing proportion of ruthenium in the structure. An annealing of the structure or application of an „anti-stress“ sublayer can be performed for compensation of internal stresses, which would have the opposite, in this case — positive, sign of internal stresses.

Conclusion

We studied the reflective and structural characteristics of multilayer X-ray mirrors in this paper based on a pair of Ru/B_4C materials. A study of the width of the transition regions showed that they are located at level 2 Å, which eliminates the need to use interface engineering to increase the reflection coefficient. The structural parameters determined in experiments allow predicting the reflectivity properties of Ru/B_4C MLMs in a wide spectral range. A study of the internal stresses of a number of samples showed that their sign has a negative value for all values of the ruthenium fraction in the period. To compensate for internal stresses, it is proposed to perform thermal annealing of structures and apply an additional „anti-stress“ sublayer, which would have the opposite sign of internal stresses.

Funding

The study was supported by the Ministry of Science and Higher Education of the Russian Federation, Agreement № 075-15-2021-1350 dated October 5, 2021 (reference number 15.SYN.21.0004).

Conflict of interest

The authors declare that they have no conflict of interest.

References

[1] A. Pirati, J. van Schoot, K. Troost, R. van Ballegoij, P. Krabbendam, J. Stoeldraijer, E. Loopstra, J. Benschop, J. Finders, H. Meiling, E. van Setten, N. Mika, J. Dredonx, U. Stamm, B. Kneer, B. Thuering, W. Kaiser, T. Heil, S. Migura. Proc. SPIE., **10143**, 101430G (2017). DOI: 10.1117/12.2261079

[2] N.I. Chkhalo, N.N. Salashchenko. AIP Advances, **3** (8), 082130 (2013). DOI: 10.1063/1.4820354

[3] Electronic media. Available at: https://www.asml.com/en/products/euv-lithography-systems

[4] N.N. Salashchenko, N.I. Chkhalo. Her. Russ. Acad. Sci., **78**, 279 (2008). DOI: 10.1134/S1019331608030155

[5] S.S. Churilov, R.R. Kildiyarova, A.N. Ryabtsev, S.V. Sadovsky. Phys. Scr., **80**, 045303 (2009). DOI:10.1063/1.3524494

[6] Otsuka, D. Kilbane, J. White, T. Higashiguchi, N. Yugami, T. Yatagai, W. Jiang, A. Endo, P. Dunne, G. O'Sullivan. Appl. Phys. Lett., **97**, 111503 (2010). DOI: 10.1063/1.3490704

[7] S. A. Garakhin, V. N. Polkovnikov, N. I. Chkhalo. Poverkhnost. Rentgenovskie, sinkhrotronnye i neytronnye issledovaniya **3**, 10 (2019) (in Russian). DOI: 10.1134/S0207352819030077

[8] A.A. Akhsakhalyan, Yu. A. Vayner, S. A. Garakhin, K. A. Elina, P. S. Zavertkin, S. Yu. Zuev, D. V. Ivlyushkin, A. N. Nechay, A.D. Nikolenko, D. E. Paryev, R. S. Pleshkov, V. N. Polkovnikov, N.. N. Salashchenko, M. V. Svechnikov, N. I. Chkhalo. Poverkhnost. Rentgenovskie, sinkhrotronnye i neytronnye issledovaniya **1**, 14 (2019) (in Russian). DOI: 10.1134/S0207352819010025

[9] J. K. Lepson, P. Beiersdorfer, J. Clementson, M.F. Gu, M. Bitter, L. Roquemore, R. Kaita, P.G. Cox, A.S. Safronova. J. Phys. B: At. Mol. Opt. Phys., **43**, 144018 (2010). DOI: 10.1088/0953-4075/43/14/144018

[10] S.S. Andreev, M.M. Barysheva, N.I. Chkhalo, S.A. Gusev, A.E. Pestov, V.N. Polkovnikov, D.N. Rogachev, N.N. Salashchenko, Yu.A. Vainer, S.Yu. Zuev. Tech. Phys., **55** (8), 168 (2010). DOI: 10.1134/S1063784210080153

[11] N.I. Chkhalo, S. Kunstner, V.N. Polkovnikov, N.N. Salashchenko, F. Schafers, S.D. Starikov. Appl. Phys. Lett., **102**, 011602 (2013). DOI: 10.1063/1.4774298

[12] P. Naujok, S. Yulin, N. Kaiser, A. Tünnermann. Proc. SPIE, **9422**, 94221K-1 (2015). DOI: 10.1117/12.2085764

[13] D.S. Kuznetsov, A.E. Yakshin, J.M. Sturm, R.W.E. van de Kruijs, E. Louis, F. Bijkerk. Opt. Lett., **40** (16), 3778 (2015). DOI: 10.1364/OL.40.003778

[14] T.D. Nguyen, R. Gronsky, J.B. Kortricht. Mat. Res. Soc. Symp. Proc., **280**, (1993). DOI: 10.1557/PROC-280-161

[15] C. Borel, C. Morawe, A. Rommeveaux, C. Huguenot, J.-C. Peffen. Proc. SPIE, **6317**, 63170I-1 (2006). DOI: 10.1117/12.678472

[16] Ch. Borel, Ch. Morawe, E. Ziegler, Th. Bigault, J.-Y. Massonnat, J.-Ch. Peffen, E. Debourg. Proc. SPIE, **5918**, 591801 (2005). DOI: doi.org/10.1117/12.613873

[17] Qiushi Huang, Yang Liu, Yang Yang, Runze Qi, Yufei Feng, I.V. Kozhevnikov, Wenbin Li, Zhong Zhang, Hui Jiang, Ling Zhang, Aiguo Li, Jie Wang, Zhanshan Wang. Opt. Express, **26** (17), 21803 (2018). DOI: 10.1364/OE.26.021803

[18] I.G. Zabrodin, B.A. Zakalov, I.A. Kaskov, E.B. Klyuenkov, V.N. Polkovnikov, N.N. Salashchenko, S.D. Starikov, L.A. Suslov. Poverkhnost. Rentgenovskie, sinkhrotronnye i neytronnye issledovaniya **7**, 37 (2013) (in Russian). DOI: 10.7868/S0207352813070202

[19] M.S. Bibishkin, N.I. Chkhalo, A.A. Fraerman, A.E. Pestov, K.A. Prokhorov, N.N. Salashchenko, Yu.A. Vainer. Nucl. Instrum. Methods Phys. Res. A, **543**, 333 (2005). DOI: 10.1016/j.nima.2005.01.251

[20] M.J. Svechnikov. Appl. Crystallogr., **53** (1), 244 (2020). DOI: 10.1107/S160057671901584X

[21] R.M. Smertin, N.I. Chkhalo, V.N. Polkovnikov, N.N. Salashchenko, R.A. Shaposhnikov, S.Yu. Zuev. Thin Solid Films, **782**, 140044 (2023). DOI: 10.1016/j.tsf.2023.140044

[22] R. Shaposhnikov, V. Polkovnikov, S. Garakhin, Y. Vainer, N. Chkhalo, R. Smertin, K. Durov, E. Glushkov, S. Yakunin, M. Borisov. J. Synchrotron Rad., **31**, 268 (2024). DOI: 10.1107/S1600577524000419

[23] V.E. Asadchikov, I.N. Bukreeva, A. Duparré, I.V. Kozhevnikov, Y.S. Krivonosov, C. Morawed, M.V. Pyatakhin, J. Steinert, A.V. Vinogradov, E. Ziegle. *Optical Metrology Roadmap for the Semiconductor, Optical, and Data Storage Industries II Proceed.* V. 4449, (2001). DOI: 10.1117/12.450102

[24] M. Bass. Handbook of Optics, **1**, 1 (1995).

Translated by A.Akhtyamov